THE AMERICAN SOCIETY OF MECHANICAL ENGINEERS
345 E. 47 St., New York, N.Y. 10017

87-GT-144

Unsteady Pressure Distributions on the Impeller Blades of a Centrifugal Pump-Impeller Operating Off-Design

K. KIKUYAMA, Associate Professor, **K. MINEMURA**, Associate Professor,
Y. HASEGAWA, Research Associate, **E. Asakura**, Research Associate,
Department of Mechanical Engineering
Nagoya University, Japan

M. MURAKAMI, Professor, Department of Mechanical Engineering
Aichi Institute of Technology, Japan

ABSTRACT

Pressure distributions on the impeller blades of a centrifugal pump were examined experimentally. The periodic pressure change caused in the suction and delivery pipes by the interaction between the rotating impeller blades and the dividing ridge of the volute casing was small. However, a noticeable cyclic change in the pressure on the blade surface was measured and related to the nonuniform pressure distribution in the volute casing at off-design flow rates. In a lower than normal range of flow rates this pressure fluctuation was largely increased near the leading edge of the blade due to the turbulent fluctuations and the flow separation from the blade surfaces. These periodic pressure changes have a large effect upon cavitation inception along the impeller periphery.

NOMENCLATURE

a	: distance along blade centerline
A_1	: area of impeller inlet (blade thickness neglected)
D	: diameter of suction and discharge pipe
p	: static pressure
Q	: rate of discharge
H	: pump head
r	: radial distance
r_1, r_2	: radius of impeller inlet and exit
s	: thickness of blade (= 10 mm)
u_2	: peripheral speed at impeller exit
θ	: circumferential position of impeller (Fig. 3)
C_p	: pressure coefficient (Eqs. (4)~(6))
σi	: predicted cavitation parameter (Eq. (10))
ϕ	: coefficient of flow rate = $Q / (A_2 u_2)$
ϕ_m	: value of ϕ at best efficiency point (= 0.140)

Subscripts

s	: suction pipe
1	: just before impeller inlet
2	: just after impeller exit

INTRODUCTION

With an increase in the industrial applications of turbomachinery, there are earnest demands for pumps of higher efficiency and suction performance. For a centrifugal pump with a volute casing, understanding the interaction between the impeller and the volute is essential to improving pump efficiency. At an off-design condition it is well known that the static pressure is not uniform along the volute spiral due to mixing losses and to the presence of the volute tongue. This nonuniform pressure along the volute results not only in a radial thrust on the impeller but also in a cyclic variation of the flow inside the impeller channels. This in turn may cause reverse flow and cavitation in the impeller(Lorett and Gopalakrishan, 1986).

There are many theoretical studies on the interaction between impeller blades and volute(Lorett et al., 1986, Imaichi et al., 1980, and Iversen et al., 1960). However, few experimental verifications have been made on the existence of the unsteady flow inside the rotating impeller. The nature of the cyclic change in the flow in the impeller passages have been left unclarified due to experimental difficulties. Using transducers mounted on the impeller, Iino and Kasai (1985) measured the pressure fluctuations in a centrifugal impeller with a vaned-diffuser, and found from frequency analysis that N(rotor speed) × Zd (number of diffuser blades) component and its harmonics are dominent in the fluctuations.

The present paper describes the results of measurements of the fluctuating pressure on the impeller blades in a volute-type centrifugal pump obtained by use of a periodic sampling method. The details of the periodically oscillating nature of the flow in the impeller channel is clarified and the occurrence of cavitation at off-design conditions is discussed.

TEST APPARATUS AND PROCEDURE

The general arrangement of the test apparatus is shown in Fig. 1. Water from a head tank is led to a pump through a straight suction pipe with a length of

Presented at the Gas Turbine Conference and Exhibition, Anaheim, California — May 31-June 4, 1987

18D (D=150 mm) and is returned to the tank. The discharge rate of the pump is measured by a nozzle installed at the inlet of the suction pipe and is regulated by a throttling valve. The suction and discharge heads are measured at stations ① and ② in Fig. 1, respectively. Measurements were made for a volute-type centrifugal pump having an inlet diameter of 150 mm and a specific speed of n_S = 280 (rpm,m^3/min, m). The dimensions and specifications of its impeller are shown in Fig. 2(a). The sectional area of volute increases linearly in the peripheral direction ($dAv/d\theta$ = 19.43 cm^2/rad).

The static pressures on the blade surfaces of the impeller, near the leading edge, were measured through small sensing orifices (P0 to P8 on the pressure side and S0 to S8 on the suction side: 1 mm diameter and 2.5 mm depth) as shown in Fig. 2(b). The pressures from the orifices were transmitted to the pressure transducers (TOYODA, PMS5) mounted on the impeller. The static pressures on the hub were also measured with sensing orifices(H0,...,H3) located on the central section of the impeller passage as shown in Fig. 2(a).

The signals from the transducers were transmitted to a stationary system by means of slip rings. The amplified analog data were digitized by an A/D converter and were stored on the disk of a micro-computer. The recording of data was started at the instant when the leading edge of the instrumented blade reached the uppermost position (on OY in Fig. 3 : θ = 0°), from which the phase angle, θ , was measured. The phase-locked pressures were sampled at 14 circumferential positions during the period of 1150 impeller rotation, which was taken from the limit of the memory size of the micro-computer.

Measurements were made at an impeller speed of 600 rpm, at which the similarity law of the pump performance was ascertained to hold as shown in Fig. 4, and no cavitation bubbles were observed inside the impeller passages. In order to secure a high frequency response of the sensing orifices, water was sufficiently degassed before the tests. First resonances of the sensing orifices and the pressure transducers are 4.1 kHz and 35 kHz, respectively.

ARRANGEMENT OF DATA

The static pressure inside the impeller channels fluctuates quasi-periodically with the impeller rotation. The pressure on a blade recorded during the time of the m-th rotation, p_m (1< m <M ; M being the total number of rotations during which data were sampled), can be expressed as a function of ϕ and θ by the following relation:

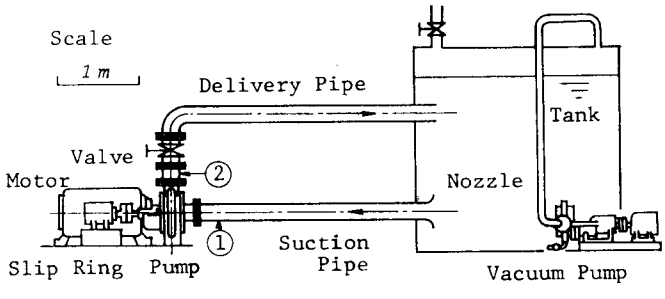

Fig. 1 Schematic outline of experimental equipment

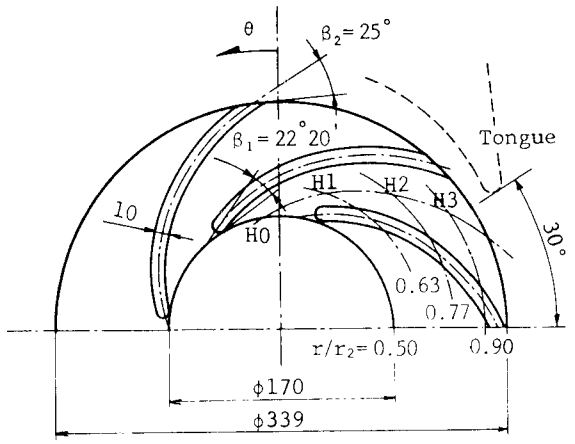

Fig. 2(a) Form and Dimensions of impeller

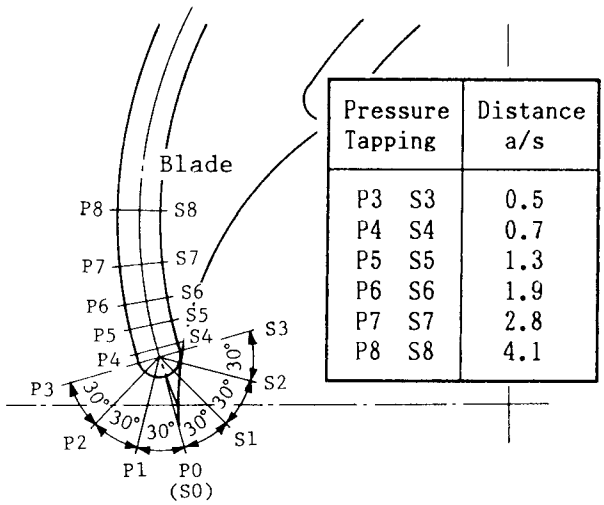

Pressure Tapping	Distance a/s
P3 S3	0.5
P4 S4	0.7
P5 S5	1.3
P6 S6	1.9
P7 S7	2.8
P8 S8	4.1

Fig. 2(b) Pressure measuring points on blade

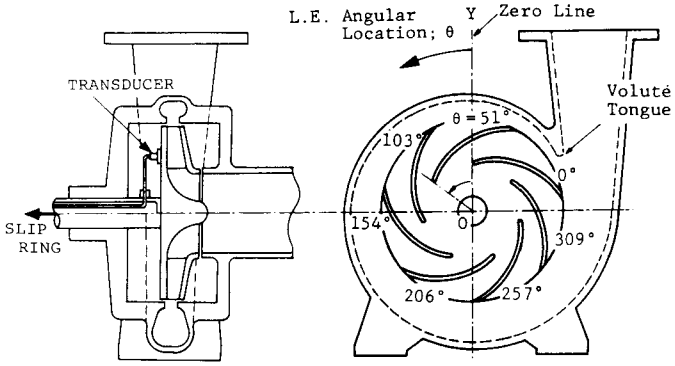

Fig. 3 Phase angles of measuring blade

$$p_m(\phi,\theta) = P(\phi,\theta) + p_m'(\phi,\theta) \quad , \tag{1}$$

where $P(\phi,\theta)$ and $p_m'(\phi,\theta)$ denote an ensemble average of the pressure and a fluctuating component with a zero average, respectively. The ensemble average is defined by :

$$P(\phi,\theta) = \frac{1}{M}\sum_{m=1}^{M} p_m(\phi,\theta) \quad . \tag{2}$$

This is obtained by use of a phase-lock averaging method (P.L.A.) which enables isolation of the periodic data from the output of the transducers. The intensity of the fluctuating component p_m' is defined by the rms value at the phase angle θ as

$$P'(\phi,\theta) = \sqrt{\frac{1}{M}\sum_{m=1}^{M}\{p_m(\phi,\theta) - P(\phi,\theta)\}^2} \tag{3}$$

The pressures obtained as above can be made dimensionless using the time mean suction pressure $\overline{P}_s$ and the peripheral speed of the impeller exit u_2, as follows:

$$C_p = \frac{\overline{P}(\phi) - \overline{P}_s}{\rho u_2^2 / 2} \tag{4}$$

$$C_p = \frac{P(\phi,\theta) - \overline{P}_s}{\rho u_2^2 / 2} \tag{5}$$

$$C_{p'} = \frac{P'(\phi,\theta)}{\rho u_2^2 / 2} \tag{6}$$

where $\overline{C}_p$, C_p and $C_{p'}$ denote the time mean, ensemble average and deviation pressure coefficients, respectively, and $\overline{P}(\phi)$ is a time-mean pressure defined as:

$$\overline{P}(\phi) = \frac{1}{2\pi}\int_0^{2\pi} P(\phi,\theta)\, d\theta \tag{7}$$

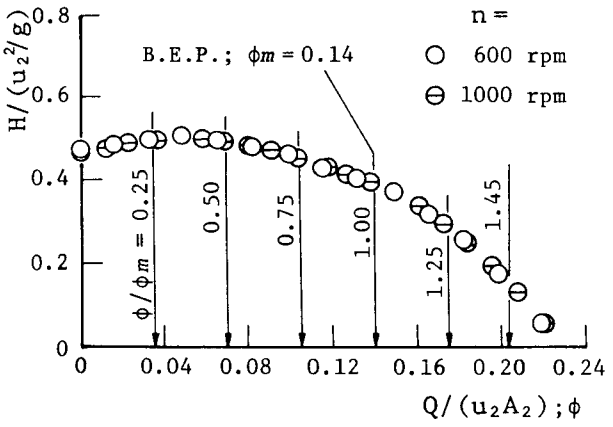

Fig. 4 Performance of Pump

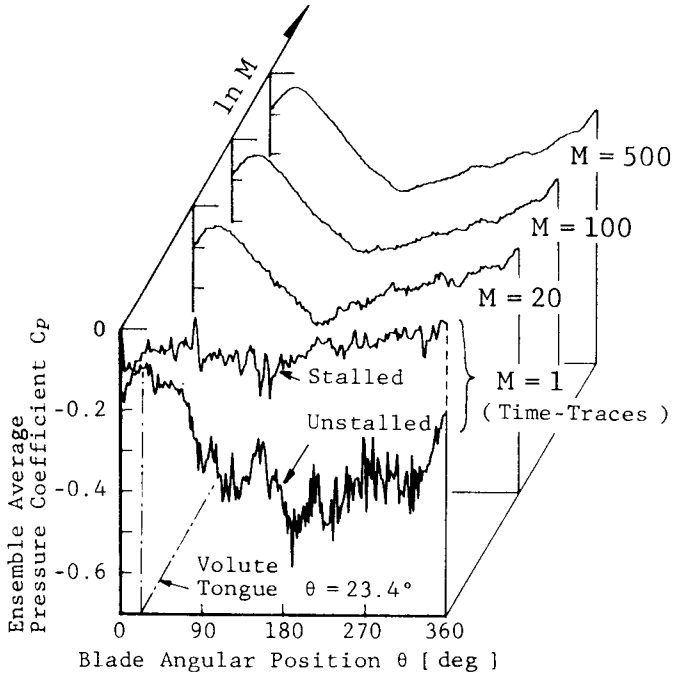

Fig. 5 Effects of number of samples on ensemble average pressure (at measuring point of S3, ϕ/ϕ_m = 0.25)

The values of $P(\phi,\theta)$ on a blade surface sampled at the rate of 256 per impeller revolution are shown in Fig. 5 (at the pressure tapping S3, ϕ/ϕ_m =0.25). Data for different values of M are compared. Compared with the time traces of the fluctuating pressure (M =1), it was found that a sufficiently smooth curve can be obtained with $M \geq 500$. On this basis, experiments were carried out with M = 1150.

UNCERTAINTIES

The uncetainty limits of the circumferential position and rotation rate were 0.5° and 1 rpm. The volumetric flow rate was measured by a suction nozzle within the uncetainty of 2 percent. The uncertain limits of the pressure coefficient derived by Eqs. (4) and (6) would be within the uncertainty of 5 percent at 20 : 1 odds.

EXPERIMENTAL RESULTS AND DISCUSSIONS

Pressure change on hub surface

Figure 6 illustrates the pressure variations on the hub surface along the circumferential direction measured at two radial locations, r/r_2 = 0.5 and 0.9, and three different flow coefficients, ϕ/ϕ_m = 0.50, 1.00 and 1.45. The value of C_{pHub} denotes the dimensionless pressure deviation from the time average static pressure coefficient, $\overline{C}_p$, and $C_{pHub} = C_p(\phi,\theta) - \overline{C}_p(\phi)$. At the radial position r/r_2 = 0.9 the pressure deviation during one rotation is small at the flow coefficient ϕ/ϕ_m =1.0, corresponding to the best efficiency point, but it increases at the other flow coefficients. At ϕ/ϕ_m = 0.5, C_{pHub} reaches its minimum when the impeller exit overlaps the volute tongue and increases with θ. At a larger flow rate, ϕ/ϕ_m = 1.45, however, C_{pHub} is at its maximum when the impeller channel passes by the volute tongue and decreases with θ. These pressure variations in the impeller passage are in good qualitative agreement with the static pressure distributions in the logarithmic spiral volute measured by A. J. Stepanoff(1957) and R. C.

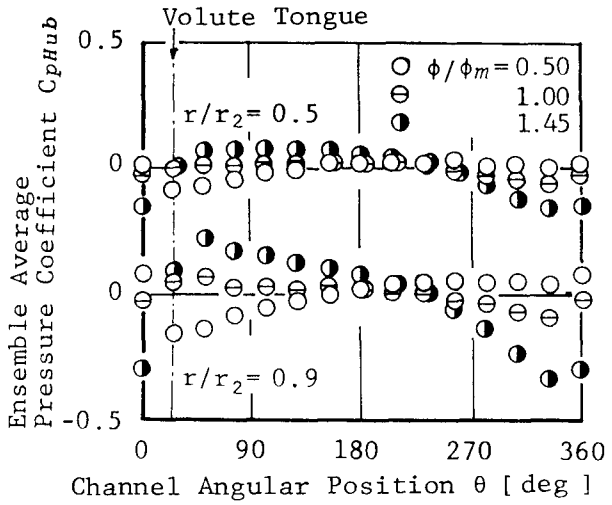

Fig. 6 Pressure variation on hub

Worster(1963). In the inlet section of the impeller channel (r/r_2 =0.5) the pressure deviations during one rotation of the impeller are less than half the size of those at r/r_2=0.9, though similarly phased circumferentially. This decrease in pressure deviation at $\phi/\phi m$ = 0.5 could be partly due to the periodic acceleration of fluid inside the passage.

Pressures on Blade Surface

Time-average pressure distributions. Figure 7 shows the distribution of the time mean pressure on a blade surface. At a low flow rate of $\phi/\phi m$ = 0.25 pre-rotation was found from the measured velocity distributions at the impeller inlet(Kikuyama et al.,

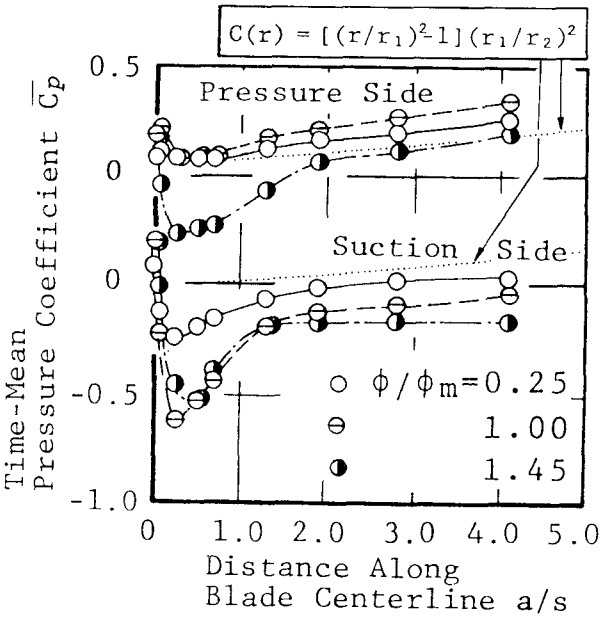

Fig. 7 Time-average pressure distributions on blade (C(r); Pressure increase due to centrifugal effect)

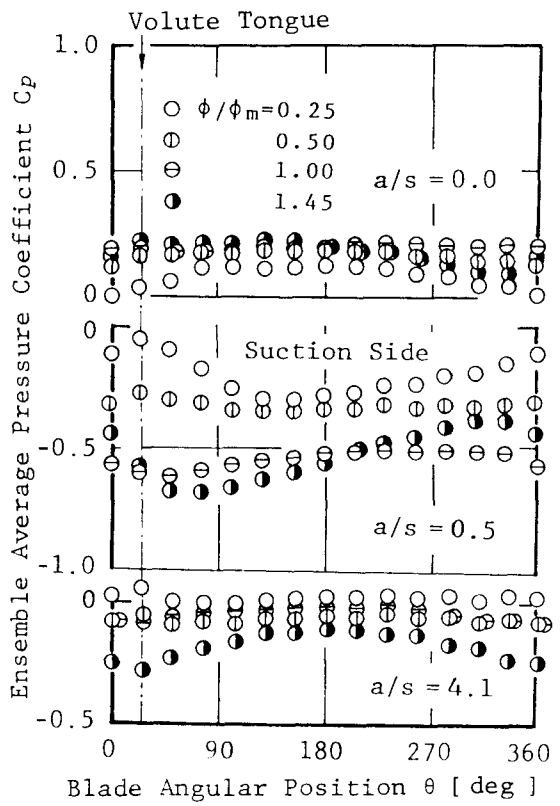

(a) suction side

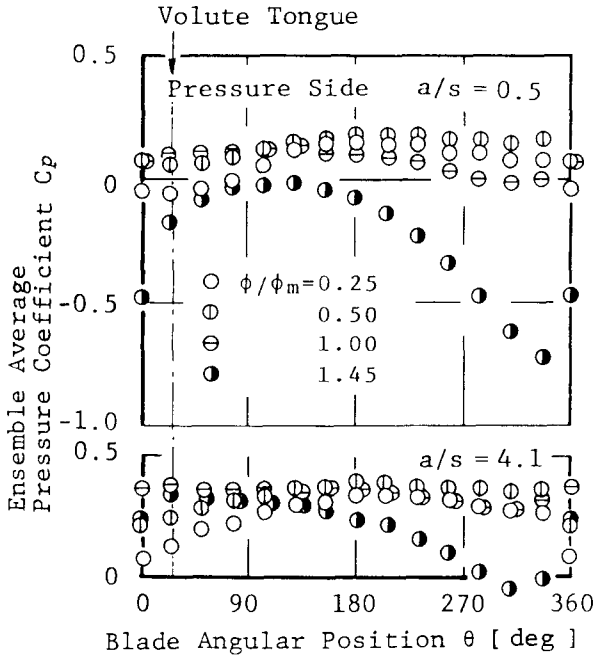

(b) pressure side

Fig. 8 Ensemble-average pressure on blade

1980). This caused a decrease in the relative velocity at the inlet and in the pressure at the leading edge. The sharp drop and the subsequent gradual increase in the pressure on the suction-side wall in Fig. 7 show where the flow separation occurs. When the flow coefficient is increased to $\phi/\phi m$ = 1.0, the pressure on the suction side decreases rapidly near the section of a/s = 0.3 and increases again further downstream. This flow rate resulted in the largest blade loading among the three flow rates used. At the flow rate $\phi/\phi m$ = 1.45 both the angle of attack and the pressure on the pressure side decreased. The dotted line C(r) in figure indicates the pressure increase due to the centrifugal effect.

Ensemble average presssure distributions. Figures 8(a) and (b) show the changes of the pressure on the suction and pressure surfaces of the blade measured along the circumference, at the points a/s = 0 (leading edge), 0.5 (P3,S3) and 4.1 (P8,S8). The pressure at the leading edge of the blade is almost constant, except for the case of $\phi/\phi m$ =0.25. However the pressures measured at P3 and S3 (a/s = 0.5) show considerable change along the circumferential direction both at $\phi/\phi m$= 0.25 and 1.45. When $\phi/\phi m$ = 0.25, the pressure on the suction side reaches its maximum at the circumferential position where the trailing edge of the blade overlaps with the dividing ridge of the volute. The pressure on the pressure side of the blade is at its maximum at θ = 180°.

When the flow rate is increased to $\phi/\phi m$ = 1.45, the pressures at a/s = 0.5 on the suction and pressure sides of the blade reach their maximum and minimum values, at θ = 129° and 77°, respectively. The large pressure change observed there is probably due to the

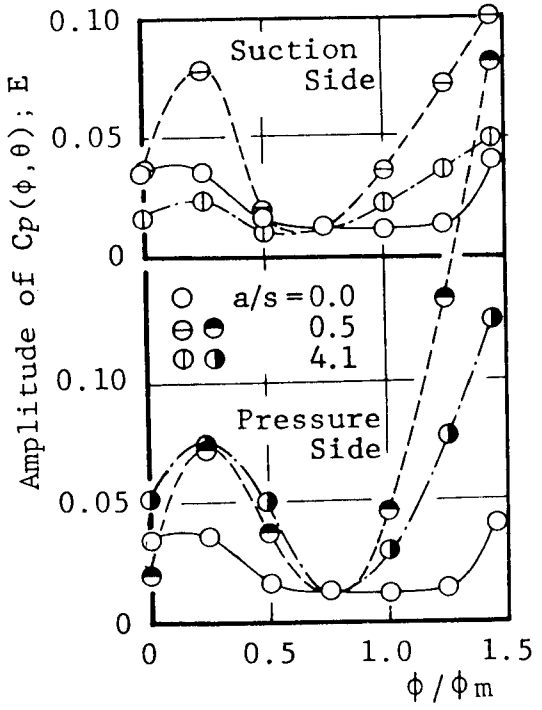

Fig. 9 Amplitude of ensemble-average pressure

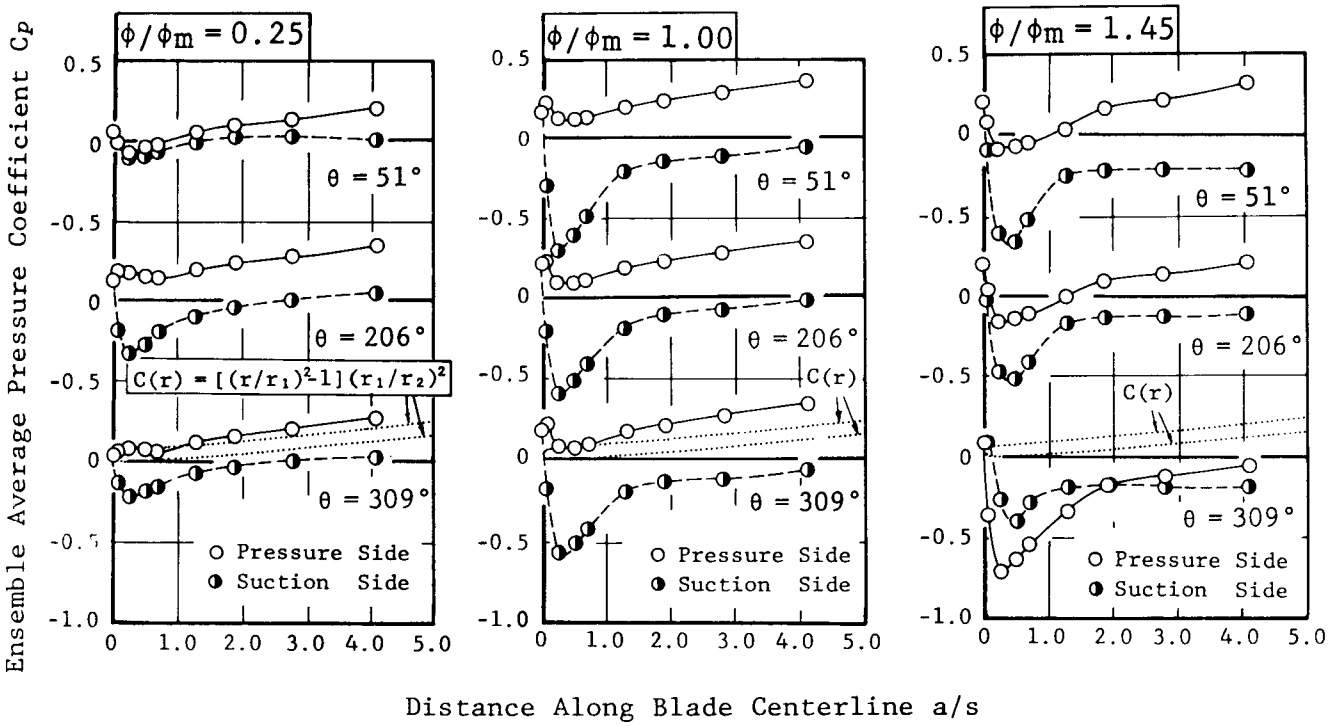

(a) $\phi/\phi m$ = 0.25 (b) $\phi/\phi m$ = 1.00 (c) $\phi/\phi m$ = 1.45

Fig. 10 Instantaneous pressure distribution on blade

asymmetric massflow distribution at the impeller inlet. At the downstream position, a/s = 4.1, the magnitude of this pressure changes decreases and the phase angle of them goes somewhat ahead.

In order to define the intensity of this pressure change, an amplitude of the ensemble mean pressure defined by the following equation is employed, and the results are shown in Fig. 9.

$$E = \frac{1}{2\pi}\int_0^{2\pi} \{Cp(\phi,\theta) - \overline{Cp}(\phi)\}^2 d\theta \qquad (8)$$

Both at $\phi/\phi m$ = 0.25 and 1.45, the value of E shows a considerable magnitude but it tends to zero at $\phi/\phi m$ = 0.75, when impeller and volute flows are best matched. Above $\phi/\phi m$ = 0.75, the value of E on the pressure side increases with the flow rate, which could be due to the effect of a large acceleration of the flow and a change in the incidence angle.

Figs. 10(a),(b) and (c) show the phase-lock-averaged pressure distributions on an impeller blade at the cicumferential locations θ = 51°, 206° and 309° , respectively. At a low flow rate of $\phi/\phi m$ = 0.25 the blade loading changes with θ and is maximum near θ = 206°. At the flow rate of the best efficiency point, however, the profiles of the pressure distributions, and therefore the blade loading remain almost unaltered during a rotation.

When the flow rate is increased to $\phi/\phi m$= 1.45, the pressure on the suction side is seen to exceed locally that on the pressure side. This is probably due to the decrease in the incident flow angle, at θ = 309°.

Turbulent pressure fluctuation. The intensity of the fluctuating pressure component Cp' at each circumferntial position is shown in Fig. 11. The pressure fluctuations both on the pressure and suction side surfaces are small at the larger flow rates, $\phi/\phi m$ = 1.0 and 1.45, for all locations. At the smaller flow rates, however, Cp' is increased both on the suction and pressure side surfaces. Cp' at a/s = 0.5 of the suction surface reaches its maximum near the circumferential position, θ = 180°, which is due to the intermittent separation of flow from the blade surface as shown in the different curves of the circumferential pressure change given in the bottom of Fig. 5.

The mean values of the pressure fluctuation intensities, $\overline{Cp'}$, observed during the period of an impeller rotation is plotted for different flow rates, in Fig. 12. The values of $\overline{Cp'}$ increase near the leading edge (a/s = 0.3) when the flow rate is reduced to $\phi/\phi m$ = 0.25, but when $\phi/\phi m$ is increased from this value, $\overline{Cp'}$ is decreased significantly. This is possibly due to the fact that the inlet flow is getting smoother as $\phi/\phi m$ is increased. The values of Cp' at a/s = 0.5 are quite comparable to those of the amplitude of the ensemble pressure fluctuation , E , shown in Fig. 9.

In order to examine the detailed nature of the pressure fluctuations, the probability density of this turbulent flow component ($p_m(\phi,\theta) - P(\phi,\theta)$) at a/s = 0.5 is shown in Figs. 13(a) and (b). As the curves of Cp' exhibit a large asymmetric nature at $\phi/\phi m$ =0.25, the probability densities had to be calculated separately for the two circumferencial ranges -26°< θ < 77° and 129° < θ < 231° . The deviation rate ($p_m(\phi,\theta)$- $P(\phi,\theta)$) devided by $P'(\phi,\theta)$ was taken as abscissa. The curves corresponding to the pressure-side wall are almost similar for both circumferential ranges, but those representing the suction side are not similar and have two peaks in the range 129°< θ < 231° and only one peak between -26° and 77°. The existence of the two

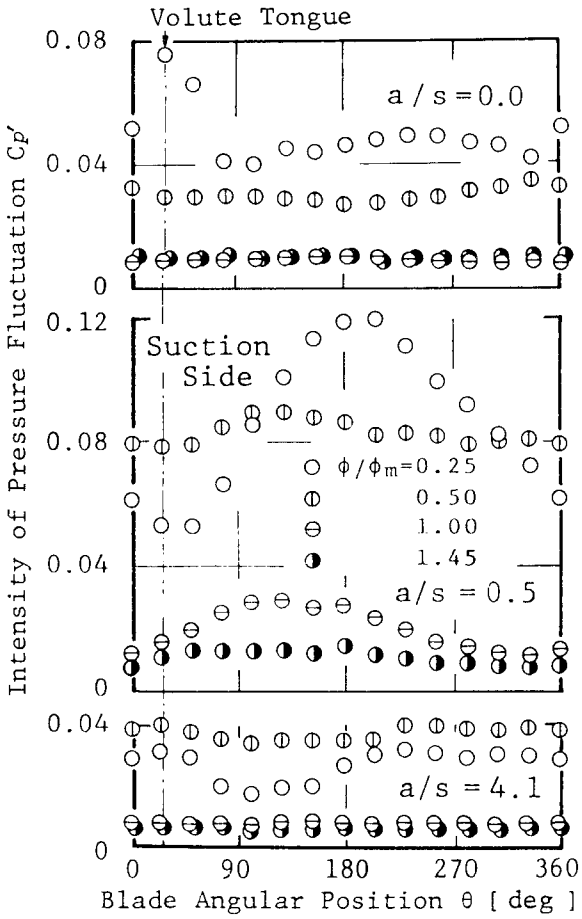

(a) suction side

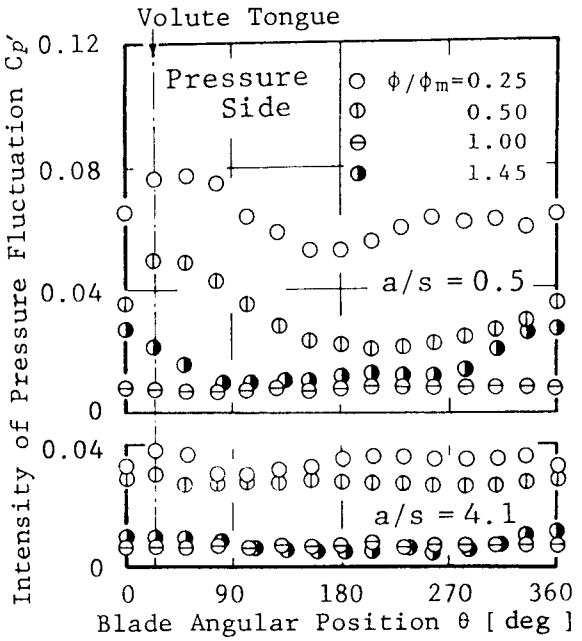

(b) pressure side

Fig. 11 Intensity of pressure fluctuation

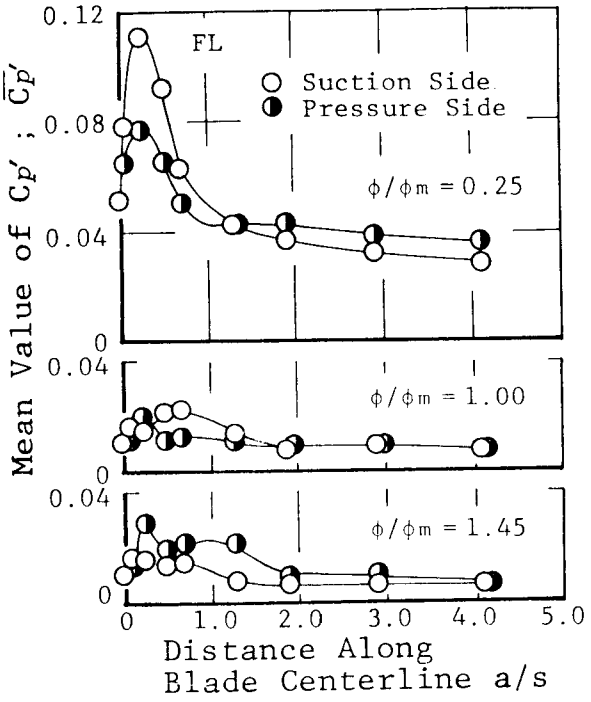

Fig. 12 Mean value of $C_{p'}$ in measured period

peaks in the probability density function is probably due to the fact that there are two quasi-stable states of the flow, that is, stalled and unstalled flow states as shown at the bottom of Fig. 5.

Figure 13(b) shows the curves of the probability function obtained during the period of a complete shaft ratation ($0° \leq \theta \leq 360°$) at the point a/s = 0.5, and for three different flow rates. When the flow rate is reduced to $\phi/\phi m = 0.5$, there is asymmetry in the curves showing an effect of the flow separation, but the curves tend to become symmetric with increasing flow rate and approach a Gaussian profile.

Cavitation Coefficient

Let the saturated vapor pressure be p_v, the cavitation coefficient is defined as follows:

$$\sigma = \frac{P_s - p_v}{\rho u_2^2 / 2} \tag{9}$$

where P_s denotes the pressure in the suction pipe. When the suction pressure P_s is decreased to P_{si}, cavitaion occurs at the position of the minimum pressure on the blade surface. Using the value of P_{si}, the incipient cavitaion coefficient σi and the local pressure coefficient C_{pmin} are given by

$$\sigma i(\phi,\theta) = (P_{si} - p_v)/(\rho u_2^2 / 2)$$

$$C_{pmin}(\phi,\theta) = (p_v - P_{si})/(\rho u_2^2 / 2)$$

$$= -\sigma i(\phi,\theta) \tag{10}$$

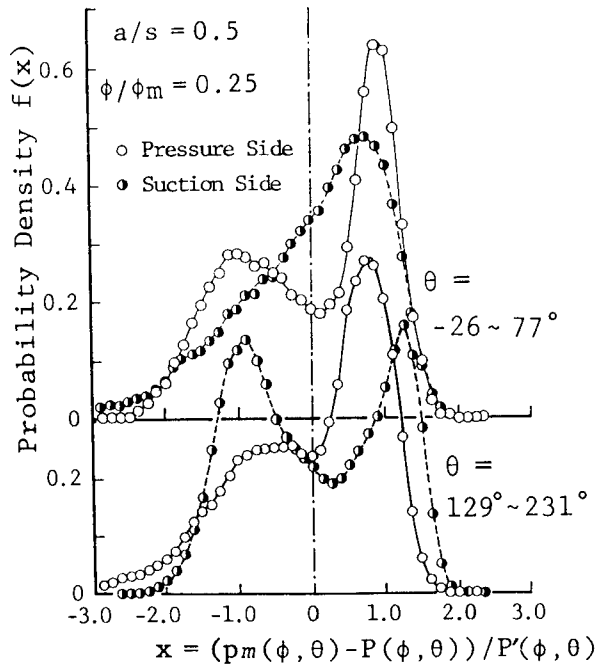

(a) $\phi/\phi_m = 0.25$

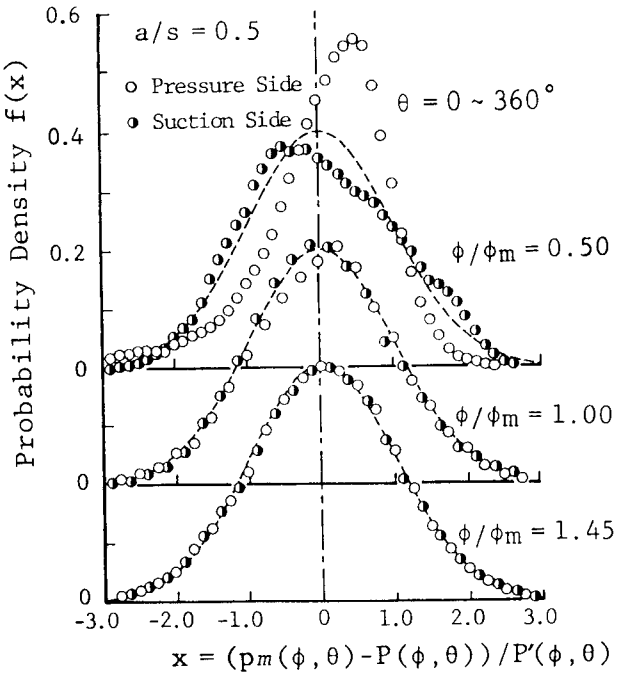

(b) $\phi/\phi_m \geq 0.5$

Fig. 13 Probability density of pressure fluctuation

Thus, the value of $\sigma i(\phi,\theta)$ can be obtained from the coefficient of the local minimum pressure $Cpmin(\phi,\theta)$ calculated from the data on the instantaneous pressure measurement.

Figure 14 shows the contours of constant σi. At a flow rate lower than $\phi/\phi m = 0.5$, the value of σi grows larger in a circumferential range of $90° < \theta < 270°$, and at a flow rate lager than $\phi/\phi m = 1.0$, it increases in the range of $0° < \theta < 180°$. Also the regions of cavitation inception observed first with the decrease in the suction head are shown in Fig. 14 (broken lines). The regions where the measured σi is maximum correspond closely to those where cavitation inception was observed. This fact shows that the circumferential changes in the pressure are closely related to the local inception of the cavitaiton on the suction-side wall.

CONCLUSIONS

For a centrifugal pump of the volute type the periodic changes in the pressure on the impeller blade and hub caused by the impeller rotation were measured and the instantaneous pressure distributions on the blade were examined at various circumferential positions along the impeller periphery. The results obtained are summarized as follows:

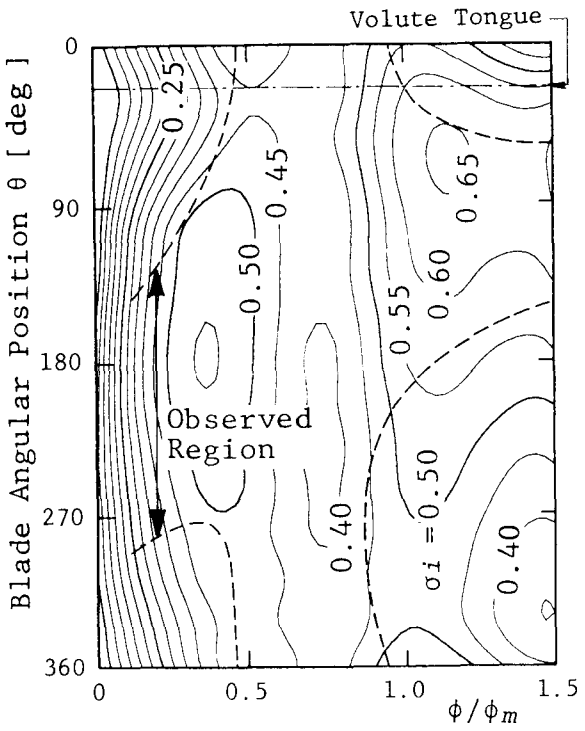

Fig. 14 Contours of cavitation parameter and observed region of cavitation (uncertainty limits of observed region ; 15°)

(1) At the flow rate of the best efficiency point the pressures on the hub and blade surfaces remain almost unchanged irrespective of the circumferential position. However, at off-design conditions these pressures change with the blade position in the pump casing, which indicates that the pressure distribution along the volute is uneven. The amplitude of the pressure changes on the hub increases near the impeller exit, while the amplitude on the blade surface shows its maximum near the leading edge.

(2) The pressure fluctuations due to turbulence near the leading edge are increased by the occurrence of the flow separation from the suction side of the blade wall.

(3) Using the minimum value of the phase-lock averaged pressure and the intensity of the pressure fluctuations on the suction-side surface, the changes in the cavitation coefficient caused by the rotation of the impeller are examined and it is ascertained that a higher value of σ_i corresponds to the circumferential position of cavitation inception.

REFERENCES

Lorett, J. A., and Gopalakrishnan, S., 1986, "Interaction Between Impeller and Volute of Pumps at Off-Design Condition, "ASME Journal of Fluids Engineering, Vol. 108, No. 1, pp.12-18.

Imaichi, K., Tsujimoto, Y., and Yoshida, Y., 1980, "A Two-Dimensional Ananysis of the Interaction Effects of Radial Impeller in Volute Casing," Proceedings of IAHR 10 th Symposium in Tokyo, Part 1, pp.635-647.

Iversen, H. W., Rolling, R. E., and Carson, J. J., 1960, "Volute Pressure Distribution, Radial Force on the Impeller, and Volute Mixing Losses of a Radial Flow Centrifugal Pump," ASME Journal of Engineering for Power, Vol. 82, No. 2, pp.136-144.

Iino, T., and Kasai, K., 1985, "An Analysis of Unsteady Flow Induced by Interaction Between a Centrifugal Impeller and a Vaned Diffuser," (in Japanese), Transactions of the Japan Society of Mechanical Engineers, Vol. 51, No. 471, pp. 154-159.

Stepanoff, A. J., 1957, "Centrifugal and Axial Flow Pumps," John Wiley.

Worster, R. C., 1963, "The Flow in Volute and its Effect on Centrifugal Pump Performance," Proceedings of Inst. Mech. Eng., Vol. 177, No. 31, pp. 843-860.

Kikuyama, K., Murakami, M., Asakura, E., and Hasegawa, Y., 1986, "Effect of Inlet Flow Pattern on Cavitaion Inception of Centrifugal Pump," Bulletine of Japan Soc. Mech. Engrs., Vol. 29, No. 254,pp. 2522-2528.